Optimum Pilot Pattern for Channel Estimation in OFDM Systems

Ji-Woong Choi, *Member, IEEE*, and Yong-Hwan Lee, *Member, IEEE*

***Abstract*—The performance of channel estimation in orthogonal frequency division multiplexing (OFDM) systems significantly depends on the pilot signal, which is usually scattered in time and frequency domains. For a given pilot density, the authors optimally design the pilot pattern so as to minimize the mean squared error (MSE) of the channel estimate with the use of a general interpolator. The analytic results are verified by computer simulation.**

***Index Terms*—Channel estimation, orthogonal frequency division multiplexing (OFDM) system, pilot pattern.**

I. Introduction

ORTHOGONAL frequency division multiplexing (OFDM) systems often employ coherent detection that requires accurate information on the channel impulse response (CIR). The CIR can be estimated using predetermined pilot symbols in real time. In the OFDM system, pilot symbols are scattered in the time and frequency domain to track time-variant and frequency-selective channel characteristics. The estimated CIR is usually interpolated for coherent demodulation of the received signal.

The interpolation can be achieved optimally using a two-dimensional (2-D) Wiener interpolator with infinite tap size. The mean squared error (MSE) of the Wiener channel estimate only depends upon the pilot density, not the pilot pattern [1]. However, it may not be practical to use such a Wiener scheme mainly due to the implementation complexity. As a result, a simple interpolator such as a linear Lagrange and Spline interpolation scheme is often employed in practice [2], [3]. When these interpolators are employed, the performance of the channel estimate is affected by the pilot pattern (i.e., the shape and spacing) as well as the pilot density [4]–[7]. For example, when the channel varies fast with a small multipath delay spread, it would be advantageous to insert more pilot symbols in the time domain than in the frequency domain, and vice versa.

There has been a number of studies on the optimal pilot pattern design for single- and multicarrier systems [4]–[13]. Optimal pilot patterns for OFDM systems were derived for time-invariant or quasi-static channels [8], [9]. The MSE of the CIR estimate is minimized, which leads to a number of equi-spaced pilot subcarriers, equal to the number of channel taps [8]. The power and the spacing of pilot subcarriers are optimized with respect to the lower bound on the average channel capacity [9]. For time-variant flat fading channels, an optimal time-domain pilot pattern with respect to the lower bound on the average channel capacity is derived [10]. Finally, an optimal pilot arrangement is constructed for packet data transmission in time-variant Rayleigh flat fading channels so as to minimize the MSE of the CIR estimate [11].

Since these schemes were designed assuming one-dimensional (1-D) channel variation, they may not provide an optimal performance when applied to 2-D signaling (i.e., in the time and frequency domain), where the relative difference of channel variation in the time and frequency domain should be considered. There has been a few studies on the design of 2-D pilot patterns in time-variant frequency-selective channels [4], [6], [7], [12]. For a given pilot density, the pilot spacing is determined in the time domain to minimize the MSE, assuming that there are as many equi-spaced pilot subcarriers as there are channel taps [12]. However, this approach may result in significant performance degradation when the CIR varies fast since a fixed number of pilot symbols are allocated in the frequency domain regardless of the channel condition. Some heuristic methods for 2-D pilot pattern design were proposed in [4], [6], and [7], where only the maximum Doppler frequency and maximum delay spread are considered to be known. However, these methods cannot provide optimal performance since they do not consider the exact distribution of the Doppler spread and power delay profile.

This paper considers the design of the optimal 2-D pilot pattern so as to minimize the MSE of the estimated CIR assuming the use of a conventional interpolator. The authors first analytically verify the optimum pilot shape that was suggested in [5] by computer simulation. For a given pilot density, the authors derive the optimal pilot spacing in terms of the moments of the Doppler spectrum and power delay profile representing the channel characteristics in the time and frequency domain, respectively.

Following the introduction, the system and channel models are described in Section II. In Section III, the optimum pilot pattern is derived for a given pilot density. The analytical design is verified by computer simulation. Finally, the concluding remarks are summarized in Section IV.

II. System Model

In an OFDM transmitter, at the nth symbol time, K data symbols $\{X[n,k]\}, k = 0,\ 1,\ 2, \ldots, K-1$, are converted into time-domain signals using the inverse fast Fourier transform (FFT). A cyclic prefix (CP) is inserted to preserve the orthogonality between the subcarriers and to eliminate the interference between the adjacent OFDM symbols.

The authors consider a wireless channel whose impulse response is represented as

$$h(t,\tau) = \sum_{l=0}^{L-1} h_l(t)\delta(\tau - \tau_l) \tag{1}$$

Manuscript received February 19, 2004; revised June 9, 2004 and August 5, 2004; accepted August 17, 2004. The editor coordinating the review of this paper and approving it for publication is G. Leus.

The authors are with the School of Electrical Engineering and INMC, Seoul National University, Kwanak, Seoul 151-600, Korea (e-mail: jwch@fruit.snu.ac.kr; ylee@snu.ac.kr).

Digital Object Identifier 10.1109/TWC.2005.853891

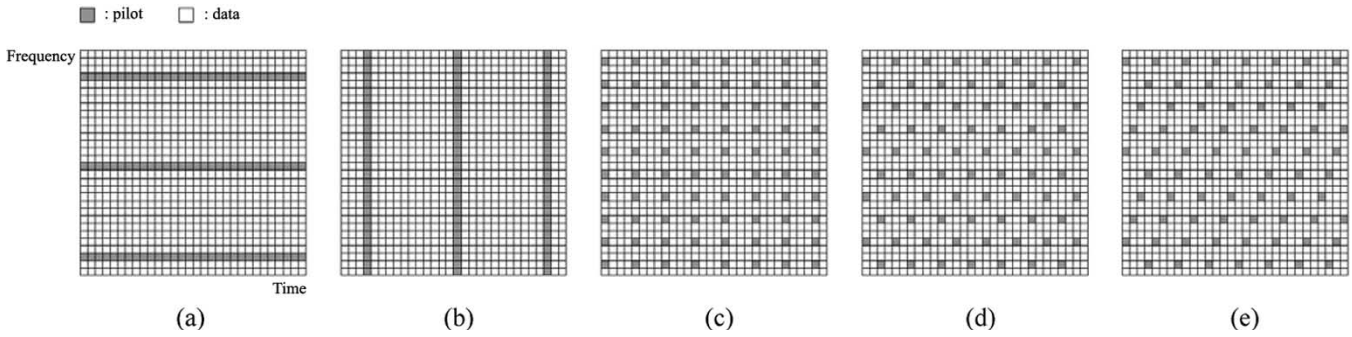

Fig. 1. Pilot arrangements on a 2-D grid.

where L is the number of paths, $\delta(\cdot)$ is the Kronecker delta function, and τ_l and $h_l(t)$ are the delay and complex-valued CIR at time t of the lth path, respectively. The authors assume that $h_l(t)$ is zero-mean Gaussian, statistically independent of each other paths and has the same normalized correlation function $r_t(\Delta t)$ for all l. Then, the time-domain correlation function of the lth path CIR can be represented as

$$r_l(\Delta t) = E\left\{h_l(t+\Delta t)h_l^*(t)\right\} = \sigma_l^2 r_t(\Delta t) \tag{2}$$

where $E\{X\}$ denotes the expectation of X, the superscript * denotes complex conjugate, and σ_l^2 denotes the average power of the lth path. The frequency response of the CIR at time t can be represented as

$$H(t,f) = \int_{-\infty}^{\infty} h(t,\tau)\mathrm{e}^{-j2\pi f\tau}\mathrm{d}\tau. \tag{3}$$

Assuming a normalized average path power (i.e., $\sum_{l=0}^{L-1}\sigma_l^2 = 1$), the correlation function of the frequency response can be represented as

$$\begin{aligned} r_H(\Delta t,\Delta f) &= E\left\{H(t+\Delta t, f+\Delta f)H^*(t,f)\right\} \\ &= r_t(\Delta t)r_f(\Delta f) \end{aligned} \tag{4}$$

where $r_f(\Delta f) = \sum_{l=0}\sigma_l^2 e^{-j2\pi\Delta f\tau_l}$. Assuming that the CIR is unchanged within the OFDM symbol period T_s, the authors can neglect the effect of intercarrier interference [6], [8]. Denoting the subcarrier spacing by Δf_c, the correlation function can be represented as

$$r_H[n,k] = r_t[n]r_f[k] \tag{5}$$

where $r_t[n] = r_t(nT_s)$ and $r_f[k] = r_f(k\Delta f_c)$. The corresponding spectrum of the channel correlation can be represented as

$$\begin{aligned} S_H(w_1,w_2) &= \sum_{n=-\infty}^{\infty}\sum_{k=-\infty}^{\infty} r_H[n,k]e^{-j(w_1 n - w_2 k)} \\ &= \sum_{n=-\infty}^{\infty} r_t[n]e^{-jw_1 n}\sum_{k=-\infty}^{\infty} r_f[k]e^{jw_2 k} \\ &= S_{H_1}(w_1)S_{H_2}(w_2) \end{aligned} \tag{6}$$

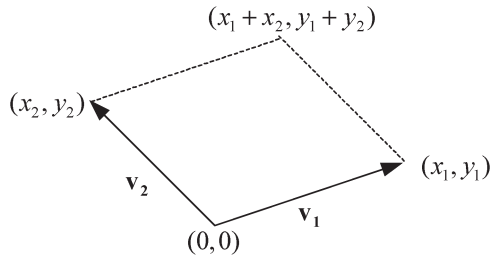

Fig. 2. Pilot pattern in Cartesian coordinates.

where $S_{H_1}(w_1)$ and $S_{H_2}(w_2)$ are the FT of $r_t[n]$ and $r_f[k]$, respectively.

At the receiver, the CP is removed before the FFT process. Assuming ideal synchronization at the receiver, the received symbol of the kth subcarrier at the nth symbol time can be represented by

$$Y[n,k] = X[n,k]H[n,k] + Z[n,k] \tag{7}$$

where $H[n,k]$ is the frequency response of the channel at the kth subcarrier and the nth symbol time, and $Z[n,k]$ is the background noise, which can be approximated as zero-mean additive white Gaussian noise (AWGN) with variance σ_z^2. The authors also assume that the signal is sampled at a rate satisfying the Nyquist sampling condition.

III. Optimum Pilot Pattern

The authors consider the use of pilot patterns with a regular structure since the use of equi-spaced and equi-powered patterns has been shown to provide better performance in addition to the simplicity of implementation [8], [11], [12]. Fig. 1 depicts various kinds of pilot patterns on a 2-D time–frequency grid in OFDM systems.

A regular pilot arrangement can be represented using two basis vectors $v_1 = [x_1, y_1]^{\mathrm{T}}$ and $v_2 = [x_2, y_2]^{\mathrm{T}}$ as shown in Fig. 2, where the vectors are represented in Cartesian coordinates: the time axis by the abscissa and the frequency axis by the ordinate. Then, all the pilot patterns with a regular structure included in Fig. 1 can be represented by using these two basis vectors. Since the pilot density D is inversely proportional to the pilot spacing, it can be defined as the inverse of the area of a parallelogram formed by v_1 and v_2, i.e.,

$$D \equiv |\det(V)|^{-1} = |x_1 y_2 - x_2 y_1|^{-1} \tag{8}$$

where $V = [v_1, v_2]$ is a (2×2) matrix representing the pilot pattern. Although x_1, x_2, y_1, and y_2 can be of any value, the authors assume $y_1 = 0$ without loss of generality since any parallelogram can be rotated such that $y_1 = 0$.

The CIR is first estimated from the pilot signal as

$$\begin{aligned}\tilde{H}[n_p, k_p] &= \frac{Y[n_p, k_p]}{X[n_p, k_p]} \\ &= H[n_p, k_p] + Z'[n_p, k_p] \end{aligned} \tag{9}$$

where n_p and k_p denote the pth symbol and subcarrier index of the pilot symbol, respectively, and $Z'[n_p, k_p]$ denotes the noise term. CIR can be estimated by interpolating the received pilot symbols as

$$\hat{H}[n,k] = \sum_{p=-\infty}^{\infty} \sum_{q=-\infty}^{\infty} \tilde{H}_s[n+p, k+q] w[p,q] \tag{10}$$

where $\tilde{H}_s[n,k]$ is equal to $\tilde{H}[n,k]$ for the pilot symbol and zero otherwise, and $w[p,q]$ denotes the coefficient of the interpolator. The authors consider the use of two 1-D interpolators for 2-D interpolation, i.e., one in the time domain and the other one in the frequency domain, to reduce the computational complexity without noticeable performance degradation [13].

When there is no interference, the CIR can be perfectly estimated using an ideal interpolator

$$H[n,k] = \sum_{p=-\infty}^{\infty} \sum_{q=-\infty}^{\infty} H_s[n+p, k+q] w_{id}[p,q] \tag{11}$$

where $H_s[n,k]$ is equal to $H[n,k]$ for the pilot symbol and zero otherwise, and $w_{id}[p,q]$ is the coefficient of an ideal 2-D brick-wall-type noncausal filter represented as [14]

$$w_{id}[p,q] = \frac{\sin\left(\frac{\pi p}{x_1}\right) \sin\left(\frac{\pi q}{y_2}\right)}{\left(\frac{\pi p}{x_1}\right)\left(\frac{\pi q}{y_2}\right)}. \tag{12}$$

Using (10) and (11), $\hat{H}[n,k]$ can be rewritten as

$$\begin{aligned}&\hat{H}[n,k] \\ &= \sum_{p=-\infty}^{\infty} \sum_{q=-\infty}^{\infty} \left(H_s[n+p, k+q] + Z_s[n+p, k+q]\right) w[p,q] \\ &\quad + \left(H[n,k] - \sum_{p=-\infty}^{\infty} \sum_{q=-\infty}^{\infty} H_s[n+p, k+q] w_{id}[p,q] \right) \\ &= H[n,k] + \sum_{p=-\infty}^{\infty} \sum_{q=-\infty}^{\infty} H_s[n+p, k+q] \\ &\quad \times \left(w[p,q] - w_{id}[p,q]\right) \\ &\quad + \sum_{p=-\infty}^{\infty} \sum_{q=-\infty}^{\infty} Z_s[n+p, k+q] w[p,q] \end{aligned} \tag{13}$$

where $Z_s[n,k]$ is equal to $Z'[n,k]$ at the pilot symbol time and zero otherwise. Note that the first term of (13) is the desired CIR, the second term is the self-distortion noise due to the use of a nonideal interpolator, and the third term is the interference due to the background noise plus interference.

The MSE of the CIR estimate can be represented as

$$\begin{aligned}\sigma_e^2 &= E\left\{ \left| \hat{H}[n,k] - H[n,k] \right|^2 \right\} \\ &= \frac{1}{(2\pi)^2} \int_{-\pi}^{\pi} \int_{-\pi}^{\pi} S_{H_s}(w_1, w_2) \left| W_e(w_1, w_2) \right|^2 dw_1 dw_2 \\ &\quad + \frac{\sigma_Z^2 D}{(2\pi)^2} \int_{-\pi}^{\pi} \int_{-\pi}^{\pi} \left| W(w_1, w_2) \right|^2 dw_1 dw_2 \\ &= \sigma_S^2 + \sigma_I^2 \end{aligned} \tag{14}$$

where σ_S^2 and σ_I^2 are, respectively, the MSE due to the self-distortion and interference, $S_{H_s}(w_1, w_2)$ is a sampled version of $S_H(w_1, w_2)$ [15]

$$\begin{aligned}S_{H_s}(w_1, w_2) &= (x_1 y_2)^{-2} \\ &\quad \times \sum_{n=0}^{x_1-1} \sum_{k=0}^{y_2-1} S_H\left(w_1 - \frac{2\pi}{x_1} n, w_2 - \frac{2\pi}{y_2} k - \frac{2\pi x_2}{x_1 y_2} n \right) \end{aligned} \tag{15}$$

and $W(w_1, w_2)$ is the 2-D FT of $w[p,q]$.

Defining the interpolation error coefficient due to the use of a nonideal interpolator as

$$w_e[p,q] = w[p,q] - w_{id}[p,q] \tag{16}$$

the authors can represent the 2-D FT of $w_e[p,q]$ as

$$W_e(w_1, w_2) = \begin{cases} W(w_1, w_2) - x_1 y_2, & |w_1| \le \frac{\pi}{x_1} \\ & \text{and } |w_2| \le \frac{\pi}{y_2} \\ W(w_1, w_2), & \text{otherwise} \end{cases}. \tag{17}$$

For example, $W(w_1, w_2)$ of a linear interpolator can be represented as [14]

$$W(w_1, w_2) = \frac{1}{x_1 y_2} \left[\frac{\sin\left(\frac{w_1 x_1}{2}\right)}{\sin\left(\frac{w_1}{2}\right)} \frac{\sin\left(\frac{w_2 x_2}{2}\right)}{\sin\left(\frac{w_2}{2}\right)} \right]^2. \tag{18}$$

Since σ_I^2 is independent of the pilot pattern, the optimum pilot pattern should be designed to minimize σ_S^2 for a given interpolator. For example, Fig. 3 depicts $S_{H_S(w_1,w_2)}$ and $|W_e(w_1, w_2)|^2$ when a linear interpolator is employed, where f_d and $\tau_{\max}$ denote the maximum Doppler frequency and maximum delay of the channel, respectively. Given x_1 and y_2, σ_S^2 depends on x_2 due to the MSE difference in

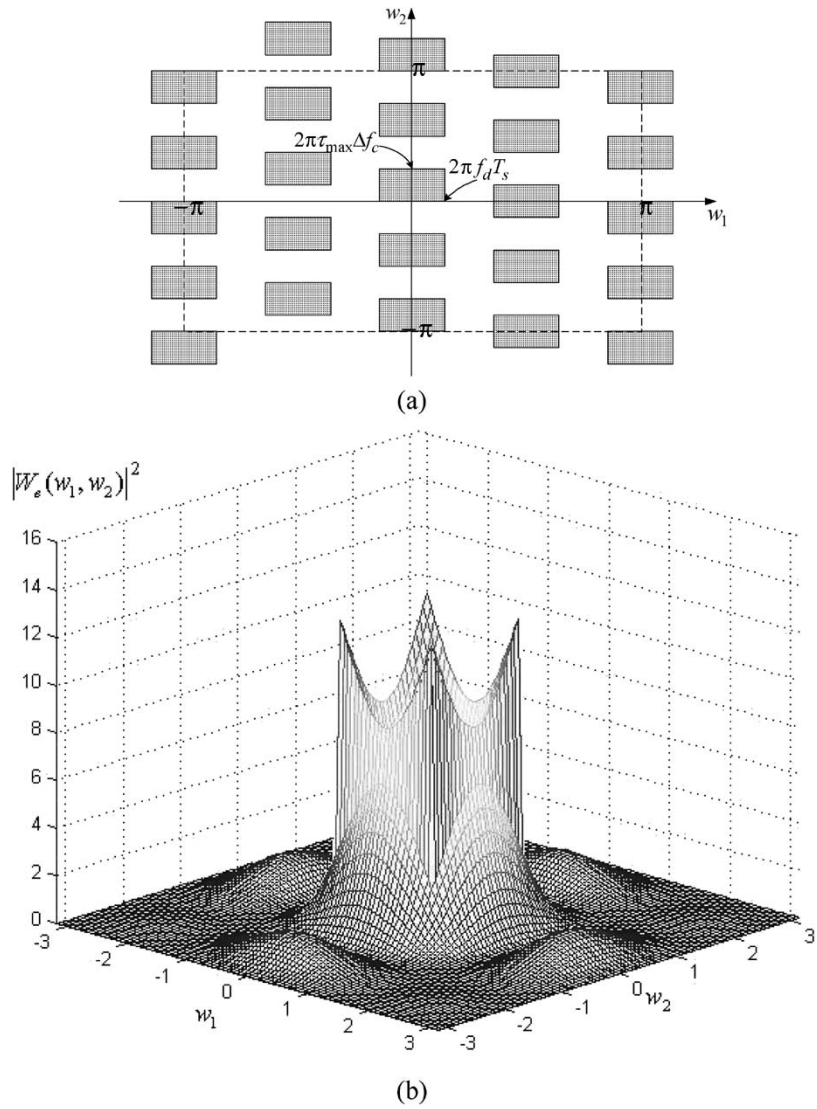

Fig. 3. 2-D spectrum of the channel correlation and interpolation error for a linear interpolator when $x_1 = y_2 = 4$ and $x_2 = 1$.

the out-of-passband spectrum (i.e., $w_1 \notin [-\pi/x_1 \ \pi/x_1]$ and $w_2 \notin [-\pi/y_2 \ \pi/y_2]$). Using the symmetrical property, it can easily be shown that σ_S^2 is minimized when $x_2 = x_1/2$. This means that the optimum pilot pattern has a diamond shape that was suggested by the simulation results in [5]. However, the variation of σ_S^2 due to x_2 is marginal since the MSE in the out-of-passband spectrum is usually much smaller than that in the passband as seen in Fig. 3(b). Note that other conventional interpolation filters have a stopband attenuation larger than the linear interpolator. Thus, the MSE in the out-of-passband spectrum can be neglected for the calculation of the MSE when other conventional interpolation filters are employed.

Neglecting the MSE in the out-of-passband spectrum and using a Taylor series approximation of $|W_e(w_1, w_2)|^2$, the authors can approximate σ_S^2 as that shown in (19) at the bottom of the page, where $\overline{w}_1^{(n)}$ and $\overline{w}_2^{(n)}$ are, respectively, the nth

$$\begin{aligned}
\sigma_S^2 &\approx \frac{1}{(2\pi)^2} \int_{-\frac{\pi}{y_2}}^{\frac{\pi}{y_2}} \int_{-\frac{\pi}{x_1}}^{\frac{\pi}{x_1}} S_{H_s}(w_1, w_2) \left(c_{IF,0} w_1^2 w_2^2 + c_{IF,1} w_1^4 + c_{IF,2} w_2^4\right) \mathrm{d}w_1 \mathrm{d}w_2 \\
&= \frac{1}{(x_1 y_2)^2 (2\pi)^2} \int_{-\pi}^{\pi} \int_{-\pi}^{\pi} S_{H_1}(w_1) S_{H_2}(w_2) \left(c_{IF,0} w_1^2 w_2^2 + c_{IF,1} w_1^4 + c_{IF,2} w_2^4\right) \mathrm{d}w_1 \mathrm{d}w_2 \\
&= (x_1 y_2)^{-2} \left(c_{IF,0} \overline{w}_1^{(2)} \overline{w}_2^{(2)} + c_{IF,1} \overline{w}_1^{(4)} + c_{IF,2} \overline{w}_2^{(4)}\right) \qquad (19)
\end{aligned}$$

TABLE I
SIMULATION CONDITIONS

Parameters	Value
FFT Size	512
Number of Subcarriers	512
Subcarrier Spacing (Δf_c)	125 kHz
Symbol Duration (T_s)	8 μs (6.4 μs +1.6 μs: guard interval)
Modulation	QPSK ($(I, Q) = 1/\sqrt{2}\,(\pm 1, \pm 1)$)
Channel	Rayleigh (Jakes' spectrum)
Tap Profile	Exponential (nine paths, 25 ns equi-spaced, power decaying factor: 2.9 dB)
Carrier Frequency	5.8 GHz
Normalized Doppler Frequency ($f_d T_s$)	0.0056
Pilot Density (D)	1/72 (1.4%)

order moment of the Doppler spectrum and power delay profile represented as

$$\overline{w}_1^{(n)} = \frac{1}{2\pi}\int_{-\pi}^{\pi} w_1^n S_{H_1}(w_1)\mathrm{d}w_1$$
$$\overline{w}_2^{(n)} = \frac{1}{2\pi}\int_{-\pi}^{\pi} w_2^n S_{H_2}(w_2)\mathrm{d}w_2 \tag{20}$$

and $c_{IF,0}$, $c_{IF,1}$, and $c_{IF,2}$ are the coefficients of the approximated polynomial of $|W_e(w_1, w_2)|^2$. Note that $\overline{w}_1^{(n)}$ and $\overline{w}_2^{(n)}$ depend on the channel correlation, but $c_{IF,0}$, $c_{IF,1}$, and $c_{IF,2}$, depend on the interpolator.

Assume that x_1 and y_2 are continuous parameters for ease of analytical design. The optimal spacing $\hat{x}_1$ and $\hat{y}_2$ can then be uniquely determined by solving

$$\left.\frac{\partial \sigma_S^2}{\partial x_1}\right|_{x_1=\hat{x}_1} = 0 \quad \text{and} \quad \left.\frac{\partial \sigma_S^2}{\partial y_2}\right|_{y_2=\hat{y}_2} = 0. \tag{21}$$

The spacing of the optimum pilot symbol should be determined by the interpolator type and the moments of the Doppler spectrum and power delay profile of the channel. As an example, consider the spacing of the optimum pilot pattern when a linear interpolator is employed for channel estimation. Assuming $x_1^2, y_2^2 \gg 1$, $c_{IF,0}$, $c_{IF,1}$, and $c_{IF,2}$ can be represented as a function of x_1 and y_2

$$c_{IF,0} = \frac{\left(x_1^2-1\right)\left(y_2^2-1\right)}{(72D^2)} \approx \frac{x_1^2 y_2^2}{(72D^2)}$$
$$c_{IF,1} = \frac{\left(x_1^2-1\right)^2}{(144D^2)} \approx \frac{x_1^4}{(144D^2)}$$
$$c_{IF,2} = \frac{\left(y_2^2-1\right)^2}{(144D^2)} \approx \frac{y_2^4}{(144D^2)}. \tag{22}$$

Thus, σ_s^2 can further be approximated as

$$\sigma_S^2 \approx \frac{2D^{-2}\overline{w}_1^{(2)}\overline{w}_2^{(2)} + \overline{w}_1^{(4)}x_1^4 + \overline{w}_2^{(4)}y_2^4}{144} \geq \frac{\overline{w}_1^{(2)}\overline{w}_2^{(2)} + \left(\overline{w}_1^{(4)}\overline{w}_2^{(4)}\right)^{\frac{1}{2}}}{72D^2} \tag{23}$$

where the equality holds when

$$\overline{w}_1^{(4)}x_1^4 = \overline{w}_2^{(4)}y_2^4. \tag{24}$$

From (24) and $D^{-1} = x_1 y_2$, the optimum spacing $\hat{x}_1$ and $\hat{y}_2$ is determined as

$$\hat{x}_1 = D^{-\frac{1}{2}}\alpha_H^{\frac{1}{8}}$$
$$\hat{y}_2 = D^{-\frac{1}{2}}\alpha_H^{-\frac{1}{8}} \tag{25}$$

where $\alpha_H = \overline{w}_2^{(4)}/\overline{w}_1^{(4)}$.

For a given pilot density, the pilot symbol should be inserted considering the ratio of the fourth-order moments of the Doppler spectrum and the power delay profile. When the mobility decreases (i.e., $\overline{w}_1^{(4)}$ decreases), it is required to increase $\hat{x}_1$ and to decrease $\hat{y}_2$. As $\overline{w}_1^{(4)}$ goes to zero, $\hat{x}_1$ goes to infinity while $\hat{y}_2$ goes to zero, resulting in a block-type pilot pattern as shown in Fig. 1(b). If $\overline{w}_1^{(4)}$ decreases (i.e., the frequency selectivity of the channel decreases), it is required to insert less pilot symbols in the frequency direction (i.e., to increase $\hat{y}_2$) and vice versa. The proposed approach can also be applied to the use of other interpolators for channel estimation. In practice, the optimum pattern can be determined by estimating the fourth-order moments of the channel spectrum that usually varies very slowly [17]. Or, it can be predetermined assuming the worst channel condition.

To verify the analytical results, the performance is evaluated by computer simulation in terms of the bit error rate (BER) when the proposed pilot pattern is used with a linear interpolator. Table I summarizes the simulation parameters of

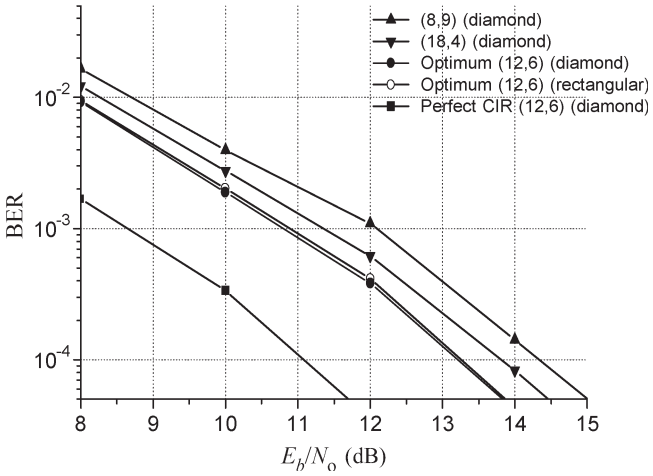

Fig. 4. BER performance for different pilot patterns with density $D = 1/72$.

the OFDM system and propagation channel [16]. For these parameters, the optimum pilot spacing is analytically determined as $(\hat{x}_1, \hat{y}_2) = (12, 6)$. For performance comparison, the authors also evaluate the performance of $(x_1, y_2) = (8, 9)$ and (18, 4), which have the same pilot density as (12, 6). Note that $(x_1, y_2) = (8, 9)$ corresponds to the pilot spacing in [12] and (18, 4) to that in [4], [6], [7]. It can be seen from Fig. 4 that the use of the proposed pilot pattern provides noticeable BER performance improvement over the use of other ones when a linear interpolator is employed. It can also be seen that the use of a diamond pattern is slightly better than the use of a rectangular pattern.

IV. Conclusion

This paper analytically determined the optimum pilot pattern for channel estimation in an OFDM system with the use of conventional interpolators. The authors have verified that the optimum pilot pattern has a diamond shape. The spacing of the pilot symbols is optimally determined in terms of the pilot density, Doppler spectrum, and power delay profile. Finally, the analytical results have been verified by computer simulation.

References

[1] Y. Li, "Pilot-symbol-aided channel estimation for OFDM in wireless systems," *IEEE Trans. Veh. Technol.*, vol. 49, no. 4, pp. 1207–1215, Jul. 2000.

[2] S. Coleri, M. Ergen, A. Puri, and A. Bahai, "Channel estimation techniques based on pilot arrangement in OFDM systems," *IEEE Trans. Broadcast.*, vol. 48, no. 3, pp. 223–229, Sep. 2002.

[3] K. F. Lee and D. B. Williams, "Pilot-symbol-assisted channel estimation for space–time coded OFDM systems," *EURASIP J. Appl. Signal Process.*, vol. 2002, no. 5, pp. 507–516, May 2002.

[4] F. Said and H. Aghvami, "Linear two dimensional pilot assisted channel estimation for OFDM systems," in *IEE Conf. Telecommunications*, Edinburgh, Scotland, Apr. 1998, pp. 32–36.

[5] M. J. F.-G. Garcia, S. Zazo, and J. M. Paez-Borrallo, "Pilot patterns for channel estimation in OFDM," *Electron. Lett.*, vol. 36, no. 12, pp. 1049–1050, Jun. 2000.

[6] J. K. Moon and S. I. Choi, "Performance of channel estimation methods for OFDM systems in a multipath fading channels," *IEEE Trans. Consum. Electron.*, vol. 46, no. 1, pp. 161–170, Feb. 2000.

[7] P. Hoeher, S. Kaiser, and P. Robertson, "Two-dimensional pilot-symbol-aided channel estimation by Wiener filtering," in *Proc. Int. Conf. Acoustics, Speech and Signal Processing (ICASSP)*, Munich, Germany, Apr. 1997, pp. 1845–1848.

[8] R. Negi and J. Cioffi, "Pilot tone selection for channel estimation in a mobile OFDM system," *IEEE Trans. Consum. Electron.*, vol. 44, no. 3, pp. 1122–1128, Aug. 1998.

[9] S. Ohno and G. Giannakis, "Capacity maximizing pilots and precoders for wireless OFDM over rapidly fading channels," in *Proc. Int. Symp. Signals, Systems and Electronics*, Tokyo, Japan, Jul. 2001, pp. 246–249.

[10] ——, "Average-rate optimal PSAM transmissions over time-selective fading channels," *IEEE Trans. Wireless Commun.*, vol. 1, no. 4, pp. 712–720, Oct. 2002.

[11] M. Dong, L. Tong, and B. M. Sadler, "Training placement for tracking fading channels," in *Proc. Int. Conf. Acoustics, Speech and Signal Processing (ICASSP)*, Orlando, FL, May 2002, pp. 2189–2192.

[12] ——, "Optimal pilot placement for channel tracking in OFDM," in *Proc. Military Communications Conf. (MILCOM)*, Anaheim, CA, Oct. 2002, pp. 602–606.

[13] R. Nilsson, O. Edfors, M. Sandell, and P. O. Borjesson, "An analysis of two-dimensional pilot-symbol assisted modulation for OFDM," in *Proc. Int. Conf. Personal Wireless Communications (ICPWC)*, Bombay, India, Dec. 1997, pp. 71–74.

[14] A. V. Oppenheim and R. W. Schafer, *Discrete-Time Signal Processing*, 2nd ed. Upper Saddle River, NJ: Prentice-Hall, 1999.

[15] D. E. Dudgeon and R. M. Mersereau, *Multidimensional Digital Signal Processing*. Englewood Cliffs, NJ: Prentice-Hall, 1984.

[16] N. Maeda, H. Atarashi, S. Abeta, and M. Sawahashi, "Throughput comparison between VSF-OFCDM and OFDM considering effect of sectorization in forward link broadband packet wireless access," in *Vehicular Technology Conf. (VTC) Fall*, Vancouver, BC, Canada, Sep. 2002, pp. 47–51.

[17] J.-W. Choi, "Design of adaptive OFDM wireless transceivers," Ph.D. dissertation, Sch. Elect. Eng., Seoul Nat. Univ., Seoul, Korea, Aug. 2004.